Published online 26 June 2013 *Nucleic Acids Research, 2013, Vol. 41, No. 16* ***7947–7959***
doi:10.1093/nar/gkt547

Structural basis for S-adenosylmethionine binding and methyltransferase activity by mitochondrial transcription factor B1

Kip E. Guja[1,2], Krithika Venkataraman[3], Elena Yakubovskaya[1], Hui Shi[1], Edison Mejia[1], Elena Hambardjieva[1], A. Wali Karzai[3] and Miguel Garcia-Diaz[1,*]

[1]Department of Pharmacological Sciences, Stony Brook University, Stony Brook, NY 11794, USA, [2]Medical Scientist Training Program, Stony Brook University Medical Center, Stony Brook, NY 11794, USA and [3]Department of Biochemistry and Cell Biology, Stony Brook University, Stony Brook, NY 11794, USA

Received September 13, 2012; Revised May 16, 2013; Accepted May 24, 2013

ABSTRACT

Eukaryotic transcription factor B (TFB) proteins are homologous to KsgA/Dim1 ribosomal RNA (rRNA) methyltransferases. The mammalian TFB1, mitochondrial (TFB1M) factor is an essential protein necessary for mitochondrial gene expression. TFB1M mediates an rRNA modification in the small ribosomal subunit and thus plays a role analogous to KsgA/Dim1 proteins. This modification has been linked to mitochondrial dysfunctions leading to maternally inherited deafness, aminoglycoside sensitivity and diabetes. Here, we present the first structural characterization of the mammalian TFB1 factor. We have solved two X-ray crystallographic structures of TFB1M with (2.1 Å) and without (2.0 Å) its cofactor S-adenosyl-L-methionine. These structures reveal that TFB1M shares a conserved methyltransferase core with other KsgA/Dim1 methyltransferases and shed light on the structural basis of S-adenosyl-L-methionine binding and methyltransferase activity. Together with mutagenesis studies, these data suggest a model for substrate binding and provide insight into the mechanism of methyl transfer, clarifying the role of this factor in an essential process for mitochondrial function.

INTRODUCTION

Mitochondria are cellular organelles responsible for the bulk of eukaryotic cellular energy production via oxidative phosphorylation. This process is strictly dependent on the coordinated expression of nearly 100 proteins that constitute the respiratory chain, which are encoded in either the nuclear or mitochondrial genome (1). Deficiencies in mitochondrial gene expression and energy production have been implicated in a variety of genetic disorders, age-related chronic diseases and the aging process itself (2). Such deficiencies may be caused by mutations in mtDNA-encoded proteins, tRNAs or ribosomal RNAs (rRNAs) as well as by mutations in nuclear-encoded respiratory chain components or regulatory factors that control mitochondrial transcription and translation (3–6). Given the role of mitochondrial dysfunction in human disease pathology, unraveling the complexities of mitochondrial gene expression that allow for coordinated cellular energy production is of significant interest.

A critical requirement for mitochondrial gene expression is proper ribosome biogenesis. This process, which is not well understood, involves several posttranscriptional RNA modifications that are thought to be crucial for ribosome assembly. Recent evidence has highlighted the importance of these modifications in mitochondria (7,8). Although several modification sites are known in both the 12S and 16S rRNAs (9), the enzymology responsible for the modifications remains unknown, with the exception of a conserved methylation in the small ribosomal subunit (10).

KsgA and Dim1 methyltransferases dimethylate two adjacent adenine residues in a stem-loop close to the 3′ end of the small-subunit rRNA in prokaryotes and eukaryotes, respectively (11,12). This modification is highly conserved in nature and is one of the few that is present in all but a few organisms (13–15). Accordingly, both the stem-loop structure and methylation events are conserved in the human 12S mitochondrial rRNA. Seidel-Rogol and colleagues elegantly demonstrated that transcription factor B1, mitochondrial (TFB1M), a member of the KsgA/Dim1 family of methyltransferases, catalyzes the analogous rRNA modification in mitochondria (10). Methylation by KsgA is related to bacterial aminoglycoside sensitivity and TFB1M activity could similarly be related to the effect of aminoglycoside antibiotics on the

*To whom correspondence should be addressed. Tel: +1 631 444 3054; Fax: +1 631 444 3054; Email: miguel.garcia-diaz@stonybrook.edu

mitochondrial ribosome and aminoglycoside-induced hearing loss (16). Consistently, aminoglycoside sensitivity in humans is often maternally inherited (17,18). Furthermore, TFB1M modulates the effects of a pathogenic mtDNA mutation linked to deafness (2,19). Hypermethylation of the 12S rRNA has been shown to underlie these effects, which were recapitulated in a mouse model (20). Other TFB1M polymorphisms are associated with reduced insulin secretion and increased risk of type II diabetes mellitus (21), further highlighting the importance of this modification for normal mitochondrial function.

Interestingly, metazoan cells contain two TFB factors, TFB1M and TFB2, mitochondrial (TFB2M). TFB2M is an essential mitochondrial initiation factor (22,23), but despite potentially having methyltransferase activity (24) does not appear to be responsible for dimethylation of the stem-loop in the 12S mitochondrial rRNA (7). Although the extent to which TFB1M participates in transcription is controversial, it has been reported to interact with both the mitochondrial RNA polymerase, POLRMT (22), and mitochondrial transcription factor A (TFAM; 25). The relevance of these interactions for the transcription process remains unknown (22,26). However, it has recently been reported that TFB1M can associate with POLRMT in a transcription-independent manner, and that this interaction can modulate the activity of TFB1M on the mitochondrial 12S rRNA (27). Hence, TFB1M might provide a regulatory link between transcriptional regulation and ribosome biogenesis (28).

Here, we report the first X-ray crystallographic structures of the mammalian TFB1M factor. Our results demonstrate the conservation of the KsgA-like fold in TFB1M, characterize the structural basis for S-adenosyl-L-methionine (SAM) binding and provide structural insight into the mechanism of rRNA methylation, helping to clarify how this protein mediates a critical process for mitochondrial gene expression.

MATERIALS AND METHODS

Protein expression and purification

Human (residues 20–396; UniProt Q9H5Q4) and mouse TFB1M (residues 1–346; UniProt Q8WVM0) were cloned into pTEV-HMBP3, allowing expression of a fusion with His-tagged maltose binding protein cleavable by Tobacco Etch Virus (TEV) protease. TFB proteins were overexpressed in Arctic Xpress *Escherichia coli* (DE3) cells (Stratagene) at 16°C for 20 h and purified using ProBond Resin (Invitrogen), followed by overnight TEV protease cleavage, Heparin and Superdex 200 size-exclusion chromatography. *Escherichia coli* KsgA (residues 1–273; UniProt P06992) was purified as previously described (29). A selenomethionine (SeMet; Sigma-Aldrich) protein derivative of TFB1M (SeMet-TFB1M) was produced by adding SeMet and the other 19 amino acids to minimal medium, and purified as for the native protein. Proteins were concentrated using a 10 000 molecular weight cutoff (MWCO) Amicon Ultra-15 device. Concentrated proteins were stored in 20 mM HEPES (pH 8.0), 200 mM KCl, 5% glycerol and 1 mM dithiothreitol (DTT).

Crystallization and structure determination

Orthorhombic (*I*222) crystals with one molecule per asymmetric unit were obtained by hanging-drop vapor diffusion (4 µl at 26 mg/ml) at 4°C for SeMet-TFB1M (resolution 2.2 Å), HighRes-TFB1M (resolution 1.8 Å) and TFB1M:SAM (resolution 2.1 Å) with 2.9 M sodium acetate (pH 7.0) as reservoir solution. TFB1M:SAM crystals were subsequently soaked in mother liquor containing 10 mM SAM for 10 h. Diffraction data for all crystals were collected on beamline X29 at the National Synchrotron Light Source (BNL, Upton, New York). All data sets were processed using XDS (30) and SCALA (31) as implemented in autoPROC (32). The SeMet-TFB1M structure was determined with Multiwavelength Anomalous Dispersion phasing (33) using intensities measured at the Se-absorption peak, inflection and high-energy remote wavelengths (Table 1). All six selenium sites were located, and initial phases were determined using SOLVE (34), followed by density modification using RESOLVE (35). Manual model building in COOT (36) using the 2.2 Å experimental map generated a nearly complete model. Refinement was carried out in PHENIX (37), and the resulting model was subsequently refined against a second higher resolution (1.8 Å) data set (HighRes-TFB1M). Data collection and refinement statistics are summarized in Table 1. R_{work} converged to 18.4% and R_{free} to 22.4%. The final model includes residues 10–328 of TFB1M, and no Ramachandran outliers, as assessed by MOLPROBITY (38). The TFB1M:SAM structure was solved with molecular replacement, using the HighRes-TFB1M structure as a model. Manual model building and adjustment was carried out in COOT (36), followed by refinement in PHENIX (37). R_{work} and R_{free} converged to 20.5 and 23.4%, respectively. The final model for TFB1M:SAM includes residues 10–327 of TFB1M, one bound SAM molecule and no Ramachandran outliers as assessed by MOLPROBITY (38).

Anisotropic diffraction of both TFB1M and TFB1M:SAM crystals was addressed by carrying out anisotropic scaling and ellipsoidal truncation using the Diffraction Anisotropy Server (39). Briefly, data residing outside an ellipse centered at the reciprocal lattice origin and having vertices at 1/1.8, 1/2.7 and 1/1.8 $Å^{-1}$ for TFB1M or 1/2.1, 1/2.7, 1/2.1 $Å^{-1}$ for TFB1M:SAM along a*, b* and c*, respectively, were removed. This treatment resulted in improved refinement statistics and electron density maps for both models.

Kasugamycin sensitivity assay

The *ksgA* gene of the *E. coli* MG1655 strain was disrupted by P_1 transduction of the *ksgA*::Kan cassette from the Keio single gene deletion library (40). The full-length *ksgA* gene was amplified from *E. coli* MG1655 genomic DNA and cloned into the pBAD24 expression vector. The KsgA Y116A variant was generated by PCR based site-directed mutagenesis and confirmed by sequencing. Plasmids encoding the human mitochondrial TFB1M (hsTFB1M) or the mouse mitochondrial TFB1M (mmTFB1M) and its variants were expressed in MG1655 *ksgA*::Kan strain in the presence of the pRARE plasmid. Antibiotics

Table 1. Data collection, phasing and refinement statistics

	SeMet-TFB1M[a]			HighRes-TFB1M[a]	TFB1M:SAM[a]
Data collection					
Space group		I222		I222	I222
Cell dimensions					
a, b, c (Å)		47.6, 99.7, 211		47.6, 101.3, 211.6	47.7, 101.7, 211.7
α, β, γ (°)		90, 90, 90		90, 90, 90	90, 90, 90
	Peak	Inflection	Remote		
Resolution (Å)	39.8–2.2 (2.24–2.20)[b]	39.8–2.2 (2.24–2.20) [b]	39.8–2.2 (2.24–2.20)[b]	33.42–2.02 (2.03–2.02)[b]	33.47–2.08 (2.088–2.081)[b]
R_{sym}	0.106 (0.676)	0.096 (0.721)	0.107 (0.796)	0.096 (0.832)	0.046 (0.606)
I / σI	29.39 (2.67)	36.23 (2.54)	36.38 (3.17)	12.12 (2.4)	22.7 (4.1)
Completeness (%)	95.8 (81.6)	95.2 (80.4)	97.8 (85.3)	99.5 (99.7)	97.8 (100)
Redundancy	13.5 (11.4)	13.4 (11.2)	13.8 (12.2)	7.0 (7.4)	7.2 (7.4)
Refinement					
Resolution (Å)				33.42–1.80	33.47–2.10
No. reflections				33 225	23 221
Completeness (%)[c]				69.2 (17.2)	76.0 (29.8)
R_{work} / R_{free}				0.1911 / 0.2280	0.2052 / 0.2336
No. atoms					
Total				2787	2708
Protein				2546	2554
SAM				–	27
Water				233	150
B-factors					
Protein				51.7	35.3
SAM				–	53.1
Water				55.0	35.5
R.m.s deviations					
Bond lengths (Å)				0.008	0.005
Bond angles (°)				1.22	0.69
PDB ID				4GC5	4GC9

[a]One crystal was used for each data set.
[b]Values in parentheses are for the highest-resolution shell.
[c]Completeness after elliptical truncation with the Diffraction Anisotropy Server.

Ampicillin (100 μg/ml), Kanamycin (50 μg/ml) and Chloramphenicol (30 μg/ml) were added to the growth medium.

Escherichia coli ΔksgA cells with or without plasmid expressing KsgA, mmTFB1M, hsTFB1M, or their indicated variants were grown overnight at 37°C in Luria Bertani broth with appropriate antibiotics. The OD_{600} of overnight cultures was adjusted to 3.5 and diluted 1:400 in Luria Bertani broth containing 0.1% arabinose and appropriate antibiotics. Freshly prepared kasugamycin (Santa Cruz Biotechnology) was added to the broth to a final concentration of 400 μg/ml. The cells were allowed to grow at 37°C, and OD_{600} of the cultures was measured after 5 h.

All experiments were performed in triplicate and analyzed for statistical significance using a two-tailed *t*-test in Prism (GraphPad Software).

RESULTS AND DISCUSSION

Human and Mouse TFB1M are functionally conserved

To investigate how the putative methyltransferase fold of TFB proteins contributes to the mitochondrial gene expression process, we decided to crystallize full-length TFB1M. Despite developing a robust purification strategy for human TFB1M (hsTFB1M), all crystallization attempts were unsuccessful. We then considered characterizing TFB1M from an alternative mammalian species. Mouse TFB1M (mmTFB1M) is essential for mitochondrial function, and mice deficient in TFB1M display a phenotype consistent with its role as a 12S rRNA methyltransferase (7). Moreover, mmTFB1M shows a high degree of sequence conservation (85% identity with the human protein; Supplementary Figure S1). We therefore decided to determine whether the mouse protein also displays rRNA methyltransferase activity and whether this activity is comparable with that of human TFB1M.

In *E. coli,* loss of KsgA activity confers resistance to the translation inhibitor antibiotic kasugamycin (41). Consistent with the evolutionary conservation of this modification, hsTFB1M was shown to be able to functionally complement an *E. coli ksgA*$^-$ mutation (10). We therefore used the same complementation strategy to study mmTFB1M. As reported previously, expression of human TFB1M restored sensitivity to kasugamycin in a *ksgA*$^-$ strain (Figure 1A). Likewise, expression of wild-type mmTFB1M resulted in significantly increased sensitivity to kasugamycin compared with a control expressing wild-type KsgA, suggesting that mouse and human TFB1M have comparable methyltransferase

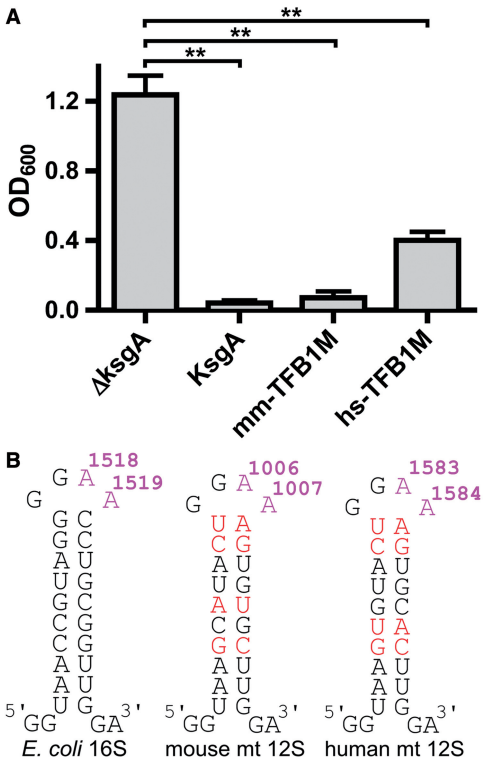

Figure 1. Functional complementation of *E. coli* KsgA rRNA methlytransferase activity by human and mouse TFB1M. (**A**) The results of a kasugamycin-sensitivity assay are shown. Plotted is the optical density (OD_{600}) after 5 h of culture growth in the presence of kasugamycin. Error bars represent the standard deviation (s.d.) of three replicates. Double asterisk indicates a *P*-value of $\leq$0.005 (see 'Materials and Methods' section). (**B**) Schematic representation of the conserved stem-loops in the 16S *E. coli* rRNA as well as the human and mouse 12S mitochondrial rRNA. The two dimethylated adenines are highlighted in magenta. Non-conserved residues are shown in red.

activities. Interestingly, mmTFB1M displayed stronger complementation activity than the human protein. Although this might be due to differential stability of the protein in bacteria, it could also be a consequence of sequence differences between the human and mouse small rRNA hairpins (Figure 1B).

Overall structure of ligand-free TFB1M

As we confirmed that mmTFB1M is a suitable model for studying the human protein, we decided to determine its crystal structure. We were able to obtain crystals of mmTFB1M that diffracted to high resolution. To facilitate phasing of the structure, we expressed and purified SeMet-substituted mmTFB1M protein from *E. coli* and obtained crystals that diffracted to a resolution of 2.0 Å (Table 1). We solved the structure using Multiwavelength Anomalous Dispersion phasing (33). The resulting electron density map was of sufficient quality to permit building of a structural model for almost all of the protein (residues 10–328; residues 1–9 and 329–346 are not resolved in the electron density). This likely includes a portion of the mitochondrial targeting peptide, as the first 13 residues of mmTFB1M are predicted to be cleaved on import into the mitochondria (42). Our X-ray crystallographic structure (Figure 2A) represents the first crystal structure of a mammalian TFB protein and definitively confirms that TFB1M shares a common fold with rRNA adenine methyltransferases. The fold displays a typical two-domain architecture (Figure 2B). The larger N-terminal domain (residues 32–236; blue in Figure 2A) that contains the putative active site forms a canonical Rossman-like methyltransferase fold with a central seven-stranded beta-sheet flanked by three α-helices on each side (Figure 2C). Two additional N-terminal α-helices (α2 and α3) and a loop region that is inserted between strands β6 and β7 define the active-site region (Figure 2D). This fold is characteristic of SAM-dependent methyltransferases (49). The smaller C-terminal domain spans residues 237–328 (yellow in Figure 2A) and consists of five α-helices (α8 to α12). TFB1M contains an additional N-terminal extension beyond the predicted methyltransferase fold. The N-terminal extension (residues 14–31; pink in Figure 2A) includes a protruding N-terminal α-helix (residues 18–31).

Comparison of the TFB1M structure with other methyltransferases reveals that the N-terminal methyltransferase core domain is relatively well conserved: RNA and DNA methyltransferases as well as small molecule methyltransferases all contain a central beta sheet surrounded by two pairs of three α-helices (Figure 2E). However, different methyltransferases present differential additions to this conserved fold. These additions are located in different positions with respect to the central core. These embellishments are likely related to the substrate specificity of the enzymes (49; Figure 2F). For instance, TFB1M contains a C-terminal addition that is also present in ErmC′, another adenine N6-specific RNA methyltransferase. Similarly, the catechol methyltransferase (COMT) contains the smallest of these additions, consistent with the small size of its substrate: the catechol molecule presumably does not require additional contacts outside the binding pocket in the core methyltransferase domain.

In addition to its C-terminal lobe, TFB1M also appears to contain an additional N-terminal α-helix that is not part of the conserved methyltransferase core or the predicted mitochondrial localization sequence. Given the peripheral position of this helix with respect to the overall fold, it is tempting to speculate that this tail might be involved in the establishment of putative protein–protein or protein–RNA interactions to help localize TFB1M to the appropriate site in the small ribosomal subunit.

A conserved pocket for SAM binding

Unlike KsgA, which does not bind SAM in the absence of the RNA substrate (51), TFB1M has been reported to directly associate with the SAM cofactor (25). In an effort to identify the structural features important for recognition and binding of the putative cofactor SAM and substrate adenine, we attempted co-crystallization and apoenzyme crystal soaks with SAM, *S*-adenosyl-L-homocysteine, 5′-methylthioadenosine (MTA; the major hydrolysis product of SAM) and adenosine

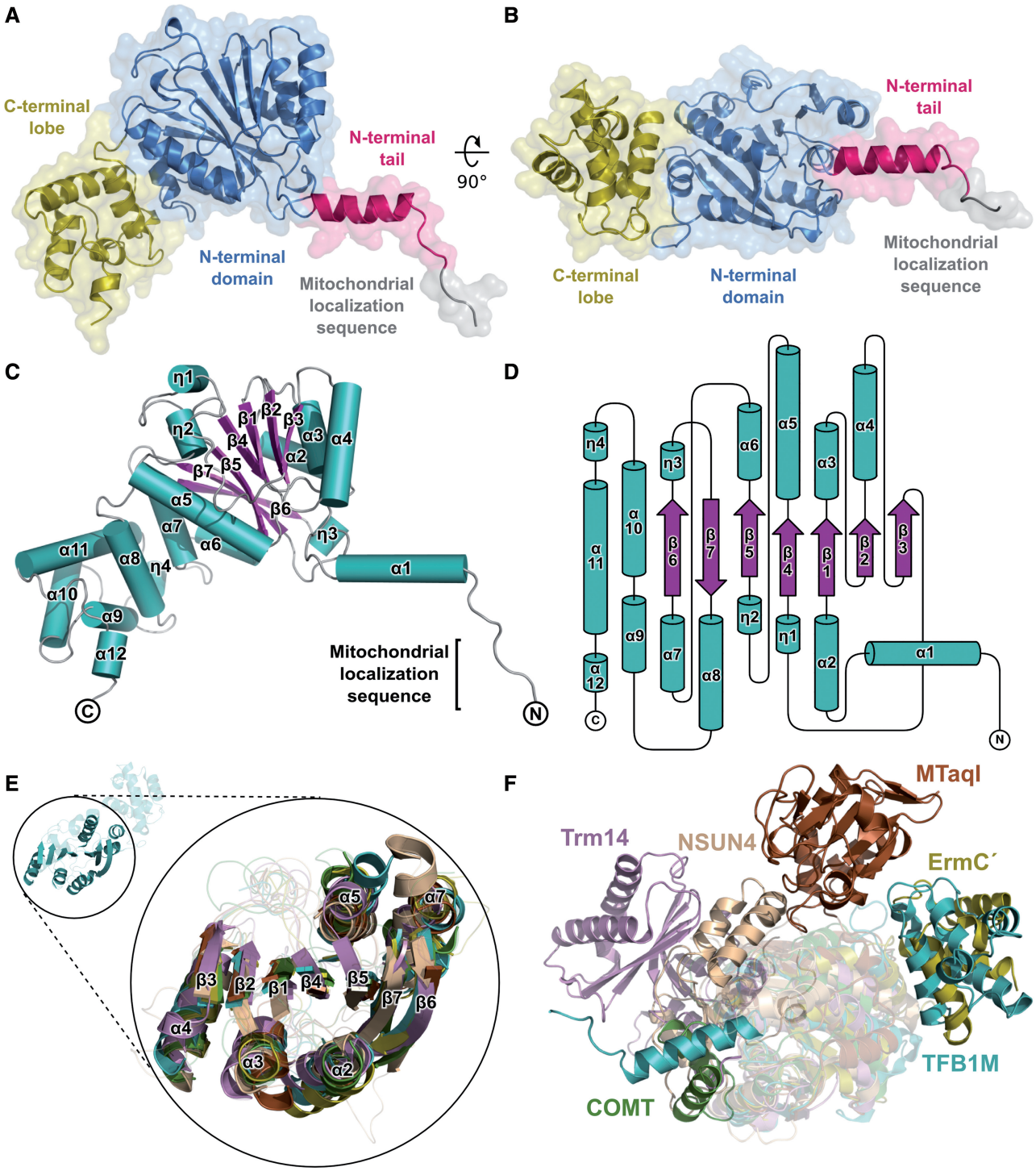

Figure 2. Overall architecture of TFB1M. (**A**) TFB1M adopts a methyltransferase fold with a two-domain architecture. A conserved N-terminal domain (blue) constitutes a Rossman-like methyltransferase fold and contains the active site. A C-terminal lobe (yellow) is believed to mediate RNA substrate specificity. A short N-terminal extension (magenta) is resolved in the crystal structure. The structure contains a portion of the mitochondrial localization sequence that is predicted to be cleaved on import (gray). The molecular surface of the protein is rendered transparent. A 90° rotation is shown in (**B**). (**C**) Schematic representation of mmTFB1M. β-strands are shown as magenta arrows, α-helices are shown as cyan ribbons and coiled regions are shown as gray lines. The N- and C-termini are marked. (**D**) Topology diagram of the protein fold using the same color coding as in (C). Secondary structure elements were identified using DSSP (43). Coiled regions are indicated by solid black lines. (**E**) Structural conservation of the methyltransferase domain. The inset shows the conservation of the central seven-stranded beta-sheet and the three flanking α-helices on each side in several classes of methyltransferases. Shown are another adenine N6-specific rRNA methyltransferase [ErmC′; yellow; PDB 1QAO; (44)], a large rRNA subunit methyltransferase [NSUN4, beige; PDB 4FZV; (45)], a tRNA methyltransferase [Trm14; pink; PDB 3TM4; (46)], a DNA methyltransferase [MTaqI; brown; PBD 2ADM; (47)] and a small-molecule methyltransferase [COMT, green; PDB 1VID (48)]. The secondary structure elements corresponding to TFB1M are labeled. (**F**) Divergence of the C-terminal lobe in different methyltransferases. The figure shows an overlay of the enzymes rendered in (E) maintaining the same color scheme. The C-terminal domain in the ErmC′ rRNA methyltransferase is similar to that in TFB1M. Other methyltransferases exhibit structurally distinct domains that are oriented differently with respect to the methyltransferase catalytic domain (see text).

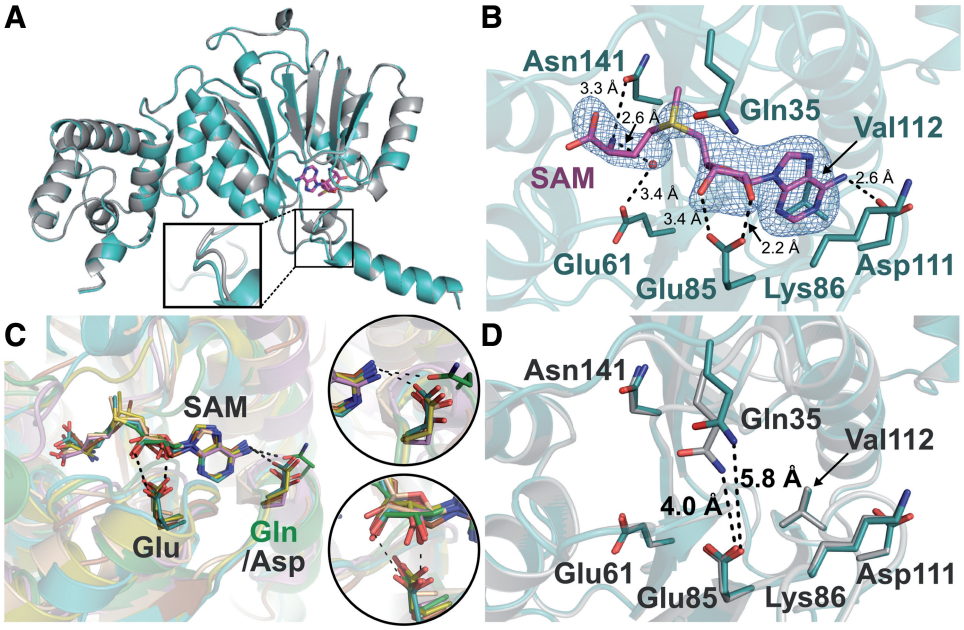

Figure 3. SAM-binding pocket in TFB1M. (**A**) Overlay between the ligand-free (gray) and SAM-bound TFB1M (cyan) structures. Both structures are essentially identical, with an rmsd of 0.26 Å for 326 C-α atoms. The inset highlights a subtle shift in the loop connecting α-helices 1 and 2 (see text). (**B**) The SAM-binding pocket in TFB1M. SAM is bound in a negatively charged binding pocket in the N-terminal domain. Several residues establish contacts with the cofactor (see text). A simulated-annealing F_o-F_c omit electron density map is shown (blue), contoured at 3σ. A water molecule (red sphere) bridges the interaction between SAM and Glu61. (**C**) Overlay of the SAM-binding pocket in the TFB1M (cyan), ErmC' (yellow), NSUN4 (beige), MTaqI (brown), Trm14 (pink) and COMT (green) methyltransferases (see Figure 2). The insets highlight two conserved interactions with the SAM cofactor. A conserved hydrogen bond with the N6 atom of the adenine base is observed in all methyltransferases (upper inset), although the protein residue involved in the interaction is not always the same and is not strictly conserved (Gln in COMT and Asp in all the others). An absolutely conserved glutamate residue forms at least one hydrogen bond to the ribose of the SAM cofactor in every structure examined (lower inset). (**D**) Overlay between the ligand-free and SAM-bound TFB1M highlighting differences in the SAM-binding pocket. The loop between α-helices 1 and 2 undergoes a subtle repositioning on SAM binding, resulting in a substantial shift of the Gln35 side chain.

monophosphate. The crystal soaks with SAM were successful, and we obtained co-crystals that diffracted to a resolution of 2.1 Å. We solved the structure of the TFB1M:SAM complex using molecular replacement with the apo-TFB1M structure as a search model. The final electron density allowed building a structural model for most of the protein (residues 10–328) and the unambiguous placement of the bound SAM molecule (Figure 3A). Data collection and refinement statistics are summarized in Table 1.

SAM is bound in a conserved acidic binding pocket in the N-terminal methyltransferase domain (Supplementary Figure S2). The structure allows us to identify several active site residues that stabilize the bound SAM molecule by a variety of hydrogen bonding and van der Waals interactions (Figure 3B). The N6 of the adenosine moiety makes a hydrogen bond to Asp 111, and the adenine base is also bracketed by van der Waals interactions with two adjacent residues, Lys 86 and Val 112. In addition, Glu85 establishes a bidentate hydrogen bonding interaction with both hydroxyl groups of the ribose. Two hydrogen-bonding interactions exist between Glu 61, Asn 141 and the amino group of the methionine moiety. Finally, the side chain carbonyl oxygen (OE1) of Gln 35 is in position to interact with the positively charged sulfur atom of the cofactor. These interacting residues are among the most highly conserved in the KsgA family [(52) Supplementary Figure S1].

The fold of the SAM-binding pocket is extremely well conserved among different methyltransferases (Figure 3C). Interestingly, this conservation is more marked in the regions of the binding pocket that contact the ribose and the adenine ring of the cofactor, whereas a greater degree of structural divergence is observed in the distal portion of the pocket, surrounding the methionine moiety (Figure 3C). As the methyl group acceptor of the substrate will need to be located in proximity to the methionine moiety, this asymmetry in the structural conservation of the pocket is likely related to the structural variability of the different substrates bound by different methyltransferases. Furthermore, the side chain interactions to the ribose and base of the nucleotide appear to be well conserved, in particular a highly conserved glutamate that interacts with the 2′ and 3′ ribose oxygens (Glu 85 for TFB1M) and a conserved interaction with the N6 atom of the adenine ring (Asp 111 for TFB1M).

Conformational change on ligand binding

To determine whether SAM binding resulted in a conformational change, we decided to compare the SAM-bound and apo TFB1M structures. The SAM-bound TFB1M structure is essentially identical to the ligand-free structure (rmsd of 0.26 Å for 318 C-α atoms; Figure 3A), implying that no large-scale conformational change takes place on SAM binding. However, closer inspection of the SAM binding pocket reveals that although SAM

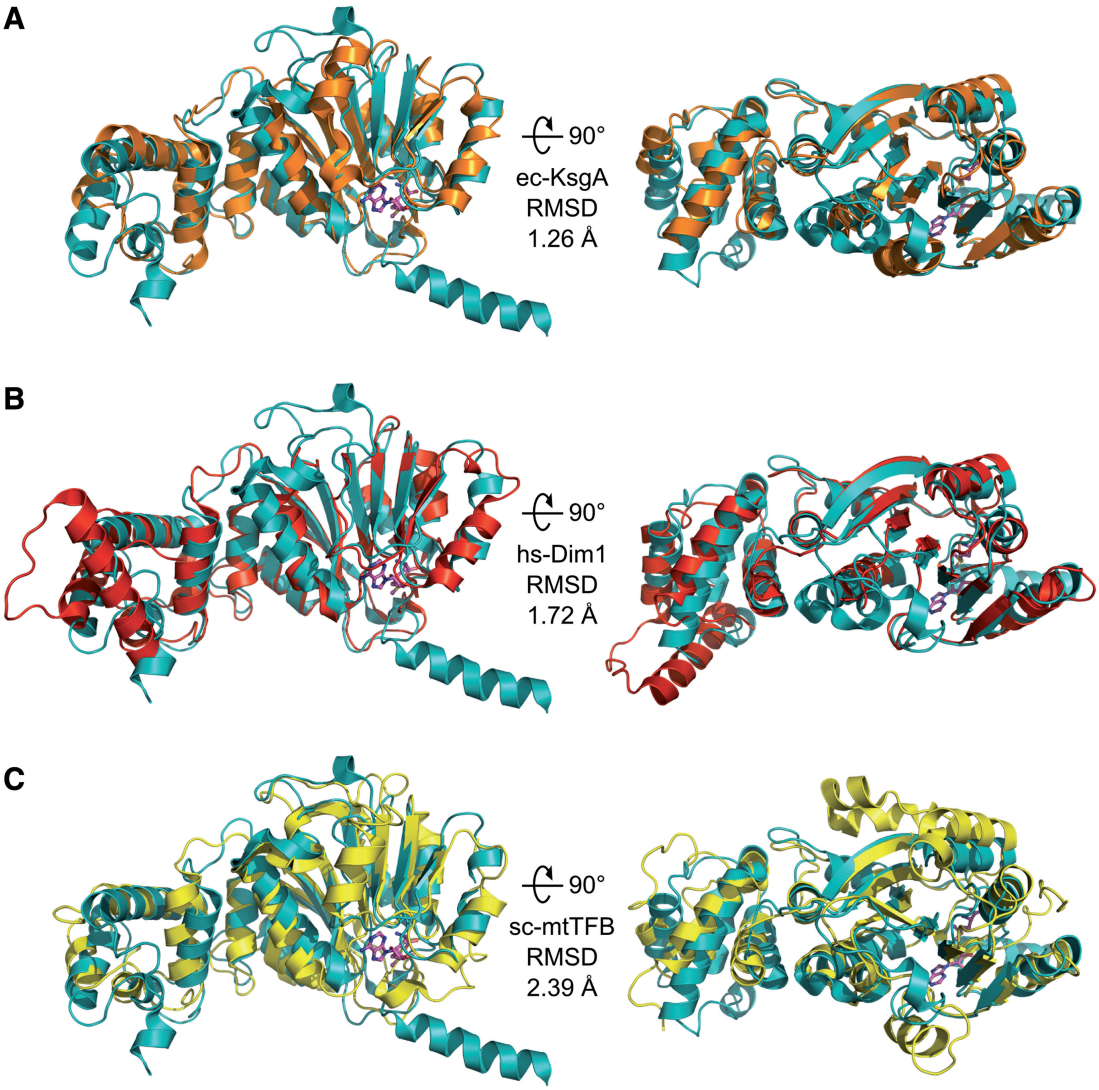

Figure 4. TFB1M is structurally similar to KsgA and Dim1 methyltransferases. (**A**) Overlay between TFB1M (cyan) and *E. coli* KsgA (orange; PDB ID 1QYR) (52). (**B**) Overlay between TFB1M and human Dim1 (red; PDB ID 1ZQ9; A. Dong, H. Wu, H. Zeng, P. Loppnau, M. Sundstrom, C. Arrowsmith, A. Edwards, A. Bochkarev and A. Plotnikov, unpublished data). (**C**) Overlay between TFB1M and sc-mtTFB (yellow; PDB ID 1I4W) (53). A 90 degree rotation is shown on the right. The SAM molecule from the TB1M structure is shown in all three panels for reference.

binding does not induce any major conformational change, slight structural perturbations are observed in the SAM-bound complex. In the apo structure, an acetate molecule is observed in the binding pocket, interacting with residues Gln35 and Glu85 (Supplementary Figure S3). On SAM binding, however, the loop containing Gln35 (which connects α-helices 1 and 2) undergoes a shift in its position (see inset in Figure 3A), effectively opening the SAM-binding pocket to accommodate the SAM molecule. This shift affects the position of Gln35, which in the apo structure is in a position that would preclude SAM from binding (Figure 3D). This type of subtle rearrangement of loop regions is typically observed in other methyltransferases (49).

TFB1M is homologous to KsgA and Dim1 proteins, but diverges from *Saccharomyces cerevisiae* mtTFB

To identify the closest structural homologs to TFB1M, we analyzed the TFB1M fold using DALI. The analysis revealed structural homology to KsgA/Dim1 proteins and to the *Saccharomyces cerevisiae* mtTFB (sc-mtTFB). Perhaps surprisingly, TFB1M exhibits the highest similarity to KsgA methyltransferases, followed by Dim1 proteins, and not with mtTFB. This is consistent with the degree of sequence identity between those proteins (25.6% with KsgA, 22.0% with Dim1 and 13.3% with mtTFB; Supplementary Figure S1) and generally in agreement with previous phylogenetic analyses (24). Comparison of the TFB1M fold with *E. coli* KsgA (rmsd of 1.26 Å for 192 C-α atoms; Figure 4A) stresses the conservation of the methyltransferase N-terminal domain: the 7-stranded β-sheet is fully conserved, as are some of the adjacent α-helices, although several divergent insertions are present in TFB1M. Nevertheless, the conservation is much lower in the C-terminal domain, perhaps emphasizing the differences between the methylation substrates in the *E. coli* and mammalian mitochondrial ribosome. A similar overlay can be produced with

human Dim1 (rmsd of 1.72 Å for 211 C-α atoms; Figure 4B), again highlighting the conservation of the N-terminal domain, although in this case, much more substantial differences exist in the C-terminal lobe, which is perhaps consistent with the larger differences that likely exist between the substrates of Dim1 and TFB1M. The subtle structural differences that exist between prokaryotic KsgA and human Dim1 might be related to the presence of additional non-methyltransferase functions in the eukaryotic enzyme (54). Interestingly, sc-mtTFB, although still maintaining a similar fold (rmsd of 2.39 Å for 212 C-α atoms; Figure 4C) is the most divergent protein of known structure in the KsgA/Dim1/TFB family. This divergence is not limited to the C-terminal lobe but is also substantial in the N-terminal domain. It is tempting to speculate that these differences may be related to the transcriptional functions of the yeast factor (54). Other methyltransferases that exhibited structural similarity to TFB1M were enzymes from the Erm family of rRNA methyltransferases (55,56) and the tRNA methyltransferase Trm14 (46,57).

Interestingly, inspection of the *E. coli* and *Thermus thermophilus* KsgA structures (58) suggests that an N-terminal α-helix, similar to that observed in TFB1M, might be present in these enzymes. This α-helix adopts a different conformation in the *T. thermophilus* structure and is not observed in the *E. coli* enzyme, but this might be due to disorder in that region of the crystal structure. When resolved in the electron density, this α-helix participates in crystal lattice contacts, and thus its conformation is likely affected by crystal packing. Hence, a similar extension might be present in other enzymes from this family.

Inspection of the electrostatic surface potential of TFB1M (Figure 5A) clearly reveals that the surface of the protein contains a large basic groove and a negatively charged binding pocket (inset in Figure 5A) where SAM binds. The large basic groove spans the entire protein fold and is likely responsible for mediating the interaction with the RNA substrate. A similar (although less markedly basic) groove is present in KsgA (Figure 5B) and yeast mtTFB (Figure 5C), suggesting that the nucleic acid binding mode might be conserved throughout the family, and stressing that the entire fold, including the C-terminal domain, appears to be involved in nucleic acid binding. Notable in the electrostatic surface potential map is the large region of positive charge in the cleft between the N-terminal and C-terminal domains. This region is present in TFB1M, KsgA and sc-mtTFB. Residues on the N-terminal side of this cleft were shown to be important for RNA binding by a similar methyltransferase, ErmC (59). However, some Erm family members, such as the *Mycobacterium tuberculosis* ermMT (60), lack the entire C-terminal domain.

Importantly, the clear acidic SAM-binding pocket that can be observed in both TFB1M and KsgA is conspicuously absent in sc-mtTFB (see insets in Figure 5). Comparison of the TFB1M and sc-mtTFB structures reveals noticeable differences around the SAM-binding pocket. Of the seven residues in TFB1M that interact directly with SAM (Gln 35, Glu 61, Glu 85, Lys86, Asp 111, Val112 and Asn 141), all appear to be conserved in KsgA (Supplementary Figure S3), human Dim1 and human TFB1M (all proteins with demonstrated methyltransferase activity), whereas only four are conserved in sc-mtTFB. Moreover, the putative SAM-binding pocket in sc-mtTFB contains several bulky side chains that are not present in the known methyltransferases and that are likely to preclude SAM binding. This is in agreement with the fact that the yeast mitochondrial ribosome does not conserve the stem-loop modification catalyzed by KsgA/Dim1/TFB proteins (15), and the observation that sc-mtTFB is unable to complement a KsgA deficiency in *E. coli* (24). Hence, the divergence of the sc-mtTFB structure is in part likely to be a consequence of the loss of its methyltransferase activity and the adaptation to facilitating transcription initiation and association with the RNA polymerase (61).

Model for substrate binding and catalysis

The major substrate of KsgA/Dim1/TFB proteins is a conserved hairpin close to the 3′ end of the small subunit rRNA (Figure 1B). The structure of the *E. coli* ribosome (62) reveals that the two nucleotides that are substrates for these proteins are located in a region of the RNA with marked single-stranded character (Figure 6A). As no catalytically relevant complexes of KsgA/Dim1/TFB proteins have been crystallized in complex with SAM and their nucleic acid substrate, we reasoned that comparisons with nucleic acid methyltransferases from other families might shed some light on the mechanism of RNA binding. The MTaqI methyltransferase is responsible for N6-adenine methylation within a double-stranded DNA TCGA sequence (63). Comparison of TFB1M with the substrate-bound complex structure of MTaqI (64) reveals that although the C-terminal domains of both proteins are divergent, consistent with the large differences in their substrates, the N-terminal catalytic domains of both enzymes are similar, with an overall rmsd of 3.9 Å for 136 C-α atoms. When the active sites are superimposed (Figure 6B), the SAM molecule bound to TFB1M and the cofactor analog bound in the MTaqI ternary complex have nearly identical orientations. Most interestingly, the substrate adenine fits into a putative substrate-binding pocket on TFB1M and displays an orientation that seems to be consistent with catalysis. Much like Tyr 108 in MTaqI is engaged in a base-stacking interaction with the substrate adenine, Phe 144 of TFB1M appears capable of forming a similar interaction with the putative substrate (Figure 6C). Significantly, this aromatic residue is conserved in KsgA/Dim1, ErmC′ (59) and other DNA methyltransferases (65).

We therefore hypothesized that TFB1M uses a binding mode that involves base flipping to gain access to the substrate adenines. Nucleic acid methyltransferases like TFB1M and MTaqI are often faced with the problem of substrate access—if the target base is involved in secondary/tertiary structure (as is common in the case of RNA), then the target base must be everted for catalysis and methylation to occur. Moreover, the electrostatic surface of TFB1M is also consistent with this binding mode,

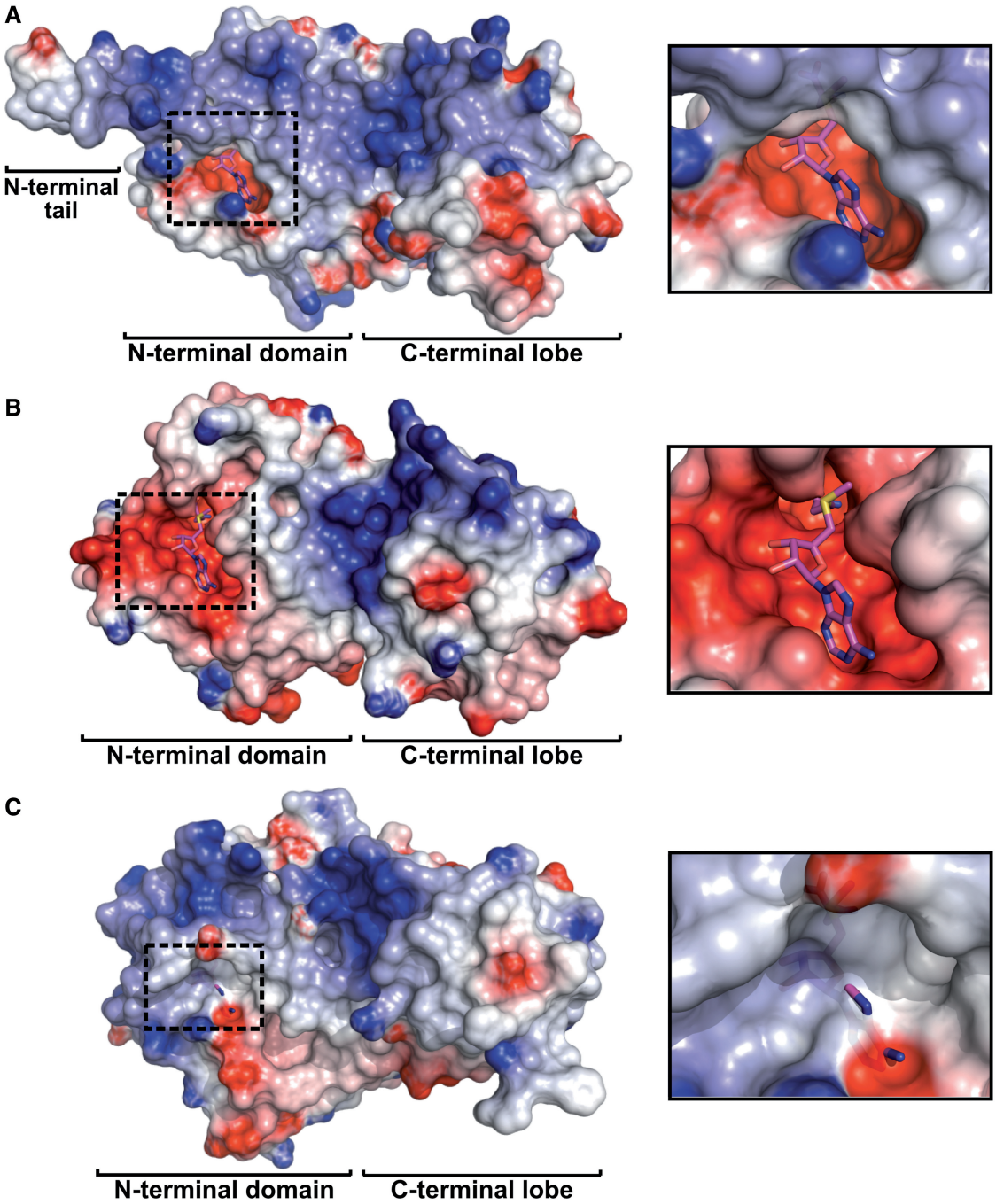

Figure 5. Electrostatic surface potential maps of TFB1M, KsgA and mtTFB. Electrostatic surface potential maps of (**A**) TFB1M in complex with SAM, shown as magenta sticks, (**B**) *E. coli* KsgA [PDB ID 1QYR] and (**C**) sc-mtTFB [PDB ID 1I4W]. The TFB1M:SAM structure was overlaid with both KsgA and mtTFB, and the SAM molecule bound in the TFB1M structure is shown in (B) and (C) for reference (magenta). The insets on the right of the figure highlight the observed SAM-bidning pocket in TFB1M and the putative SAM-binding pockets in KsgA and mtTFB. The position of the N-terminal and C-terminal domains (and the N-terminal extension for TFB1M) is indicated. The electrostatic surface potential maps were generated with Delphi (50) and are colored from -7 kTe^{-1} (blue) to $+7$ kTe^{-1} (red).

showing a positively charged groove that could interact with the RNA backbone (Figure 6D).

To further investigate the validity of this model, we generated TFB1M mutants and studied their ability to complement a KsgA deficiency. We first decided to eliminate the benzene ring of Phe 144. This ring would presumably stabilize the everted nucleotide in the active site by forming a π-stacking interaction with the adenine base. Consistently, a F144A mutant was significantly impaired in its ability to rescue the phenotype of a *ksgA*$^{-}$ strain. This result was consistent with the effect of an analogous substitution in KsgA (Y116A), indicating that this conserved aromatic residue plays an important catalytic role (Figure 6E). Furthermore, we decided to test the

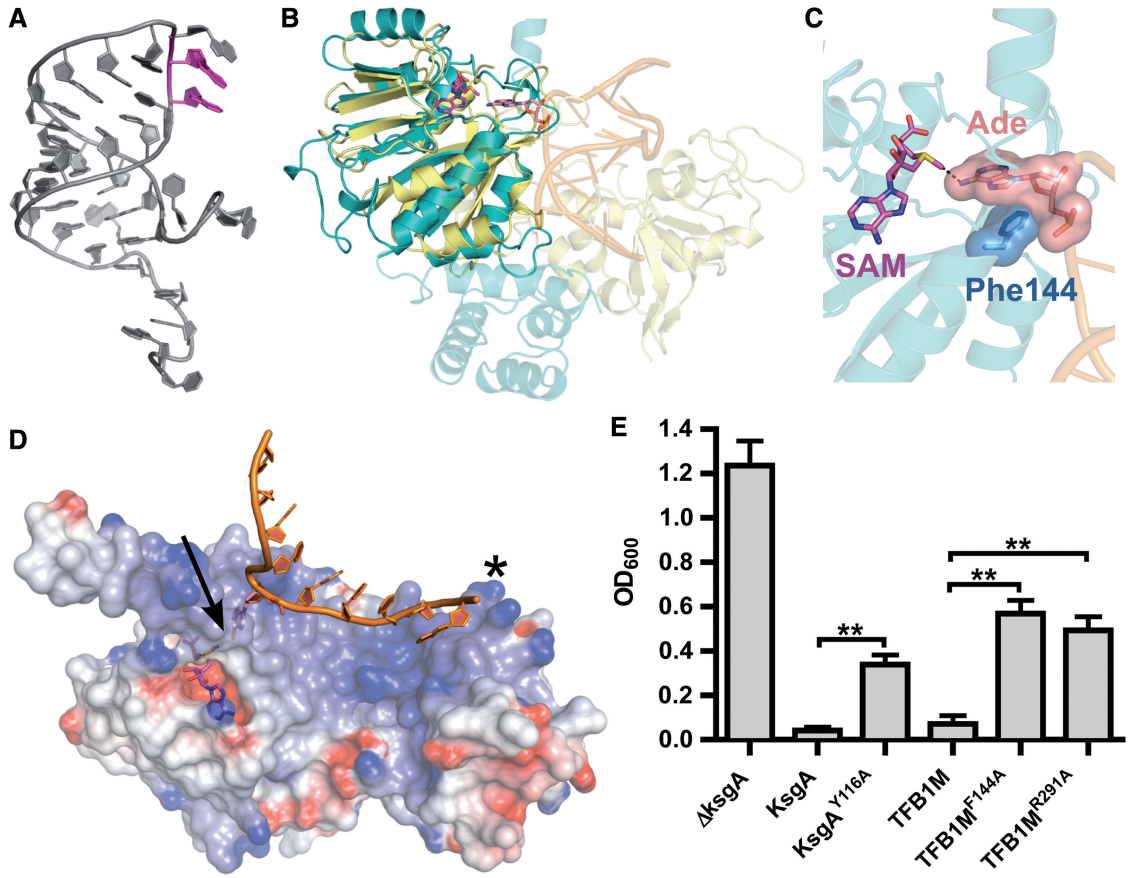

Figure 6. A model for RNA binding by TFB1M. (**A**) Structure of the conserved stem-loop in the *E. coli* 16S rRNA that is methylated by KsgA. The two substrate adenine bases are shown in magenta. (**B**) Overview of the TFB1M:SAM structure superposed with the structure of MTaqI in complex with substrate DNA and a cofactor analog [PDB entry 1G38]. TFB1M is shown in teal, with the bound SAM molecule and substrate adenine shown as magenta and pink sticks, respectively. MTaqI is shown in yellow, with the bound DNA shown in orange. The conserved methyltransferase domain of each protein is shown as a solid cartoon, whereas the remainder of each protein and the DNA is transparent. (**C**) The putative catalytic center of TFB1M. The overlay of TFB1M and MTaqI suggests a putative substrate binding mechanism that involves base flipping, with the substrate adenine residue (pink) forming a π-stacking interaction with residue Phe144 (blue) of TFB1M. The methyl leaving group of SAM and N6 of the substrate adenine are separated by a distance of 2.4 Å (dashed line). (**D**) Model for RNA binding by TFB1M. The electrostatic surface potential of TFB1M is rendered transparent, and a single DNA strand containing the substrate adenine from the MTaqI structure is shown in orange. The black arrow indicates where the methyl group of SAM and the N6 of the adenine come into close proximity. The black asterisk denotes the location of Arg291 near the backbone of the nucleic acid. (**E**) Phe144 and Arg291 are important for catalysis, suggesting that they play a role in substrate binding. The results of a kasugamycin-sensitivity assay, with optical density (OD_{600}) after 5 h of culture growth in the presence of kasugamycin is plotted in gray. The experiments were carried out using mouse TFB1M. Error bars represent the s.d. of three replicates. Double asterisk indicates a *P*-value of ≤0.005.

importance of Arg 291, a residue in the C-terminal domain that appears to be involved in forming the positively charged cleft in TFB1M. The analogous KsgA residue (Arg248) has been shown to be important for substrate binding in KsgA (66). Significantly, substitution of this residue also led to an impaired ability to complement the KsgA deficiency, indicating that the C-terminal domain is likely involved in RNA binding. This is consistent with both our model and with EM docking studies of KsgA binding to the bacterial ribosome (66).

CONCLUSIONS

TFB proteins belong to a large superfamily of methyltransferases that mediate a highly conserved rRNA modification near the 3′ end of the small ribosomal subunit. In prokaryotes, this modification is catalyzed by KsgA proteins, whereas in eukaryotes, Dim1 proteins catalyze the modification in the cytoplasmic ribosome and the mitochondrial ribosome of plants (12,13,67). The TFB branch is present in fungal and animal mitochondria (24). Its function appears to be essential for mitochondrial function in mammals (7,28) and has been implicated in the pathogenesis of different human disorders (2). In fungi and animals, this gene family has evolved an additional function related to the initiation of transcription. The two mammalian TFB proteins thus appear to unevenly distribute both functions, with TFB1M acting primarily as a KsgA-like methyltransferase and TFB2M as a transcription initiation factor. A similar functional distribution might take place in invertebrates (68–70). However, sc-mtTFB appears to have completely lost its methyltransferase activity and remain solely as a transcription factor, as the rRNA modification is not

conserved in the yeast mitochondrial ribosome (24). Accordingly, sc-mtTFB is unable to complement a KsgA deficiency in *E. coli* (24). Consistently, sc-mtTFB appears to be the most structurally divergent member of the family, whereas mammalian TFB1M is structurally and functionally more closely related to bacterial KsgA. On the other hand, there are reports that both mammalian TFB factors, TFB1M and TFB2M, act as methyltransferases—they both have the capacity to bind SAM, the methyl donor for the methyltransferase reaction, and expression of either protein can complement bacteria lacking KsgA (10,24). The extent to which TFB2M functions as a methyltransferase *in vivo* is however not well understood.

As shown here, KsgA/Dim1/TFB proteins likely take advantage of a nucleic acid binding mechanism that involves base flipping. Although our results do not yet confirm such a mechanism, the fact that the methyltransferase activities of TFB1M and KsgA depend on a conserved aromatic residue proposed to stack with the flipped out base supports this notion. Moreover, base flipping has been demonstrated for several DNA methyltransferases, such as MTaqI (71), HhaI (72) and EcoRI (73), and has been proposed as a general mechanism for nucleic acid methyltransferases (74). It would therefore not be surprising if a similar mechanism was used by the KsgA/Dim1/TFB family of rRNA methyltransferases.

ACCESSION NUMBERS

The atomic coordinates for ligand-free TFB1M and TFB1M:SAM have been deposited in the Protein Data Bank with accession codes 4GC5 and 4GC9, respectively.

SUPPLEMENTARY DATA

Supplementary Data are available at NAR Online: Supplementary Figures 1–3.

ACKNOWLEDGEMENTS

The authors thank Dr Michael Sawaya for helpful advice regarding the Diffraction Anisotropy Server and the NSLS Macromolecular Crystallography group for beamline support.

FUNDING

NSLS beamlines ×25 and ×29 are mainly supported by the Offices of Biological and Environmental Research and of Basic Energy Sciences of the US Department of Energy, and the National Center for Research Resources of the National Institutes of Health (NIH); NIH [F30-ES022930 to K.E.G., R01-GM065319 to A.W.K., R00-ES015421 and R01-GM100021 to M.G.-D.]; United Mitochondrial Disease Foundation [59042 to M.G.-D.]. Funding for open access charge: NIH [R01-GM100021 to M.G.-D.].

Conflict of interest statement. None declared.

REFERENCES

1. Ryan,M.T. and Hoogenraad,N.J. (2007) Mitochondrial-nuclear communications. *Annu. Rev. Biochem.*, **76**, 701–722.
2. Shutt,T.E. and Shadel,G.S. (2010) A compendium of human mitochondrial gene expression machinery with links to disease. *Environ. Mol. Mutagen.*, **51**, 360–379.
3. Zhu,X., Peng,X., Guan,M.X. and Yan,Q. (2009) Pathogenic mutations of nuclear genes associated with mitochondrial disorders. *Acta Biochim. Biophys. Sin.*, **41**, 179–187.
4. Ylikallio,E. and Suomalainen,A. (2012) Mechanisms of mitochondrial diseases. *Ann. Med.*, **44**, 41–59.
5. Tuppen,H.A., Blakely,E.L., Turnbull,D.M. and Taylor,R.W. (2010) Mitochondrial DNA mutations and human disease. *Biochim. Biophys. Acta*, **1797**, 113–128.
6. Copeland,W.C. (2008) Inherited mitochondrial diseases of DNA replication. *Annu. Rev. Med.*, **59**, 131–146.
7. Metodiev,M.D., Lesko,N., Park,C.B., Camara,Y., Shi,Y., Wibom,R., Hultenby,K., Gustafsson,C.M. and Larsson,N.G. (2009) Methylation of 12S rRNA is necessary for *in vivo* stability of the small subunit of the mammalian mitochondrial ribosome. *Cell Metab.*, **9**, 386–397.
8. Camara,Y., Asin-Cayuela,J., Park,C.B., Metodiev,M.D., Shi,Y., Ruzzenente,B., Kukat,C., Habermann,B., Wibom,R., Hultenby,K. *et al.* (2011) MTERF4 regulates translation by targeting the methyltransferase NSUN4 to the mammalian mitochondrial ribosome. *Cell Metab.*, **13**, 527–539.
9. Liu,J., Wang,W., Shin,D.H., Yokota,H., Kim,R. and Kim,S.H. (2003) Crystal structure of tRNA (m1G37) methyltransferase from Aquifex aeolicus at 2.6 A resolution: a novel methyltransferase fold. *Proteins*, **53**, 326–328.
10. Seidel-Rogol,B.L., McCulloch,V. and Shadel,G.S. (2003) Human mitochondrial transcription factor B1 methylates ribosomal RNA at a conserved stem-loop. *Nat. Genet.*, **33**, 23–24.
11. O'Farrell,H.C., Xu,Z., Culver,G.M. and Rife,J.P. (2008) Sequence and structural evolution of the KsgA/Dim1 methyltransferase family. *BMC Res. Notes*, **1**, 108.
12. Lim,K., Zhang,H., Tempczyk,A., Bonander,N., Toedt,J., Howard,A., Eisenstein,E. and Herzberg,O. (2001) Crystal structure of YecO from Haemophilus influenzae (HI0319) reveals a methyltransferase fold and a bound S-adenosylhomocysteine. *Proteins*, **45**, 397–407.
13. Michel,G., Sauve,V., Larocque,R., Li,Y., Matte,A. and Cygler,M. (2002) The structure of the RlmB 23S rRNA methyltransferase reveals a new methyltransferase fold with a unique knot. *Structure*, **10**, 1303–1315.
14. Bujnicki,J.M. (2001) In silico analysis of the tRNA:m1A58 methyltransferase family: homology-based fold prediction and identification of new members from Eubacteria and Archaea. *FEBS Lett.*, **507**, 123–127.
15. Dlakic,M. (2001) Chromatin silencing protein and pachytene checkpoint regulator Dot1p has a methyltransferase fold. *Trends Biochem. Sci.*, **26**, 405–407.
16. Guan,M.X. (2011) Mitochondrial 12S rRNA mutations associated with aminoglycoside ototoxicity. *Mitochondrion*, **11**, 237–245.
17. Hu,D.N., Qui,W.Q., Wu,B.T., Fang,L.Z., Zhou,F., Gu,Y.P., Zhang,Q.H., Yan,J.H., Ding,Y.Q. and Wong,H. (1991) Genetic aspects of antibiotic induced deafness: mitochondrial inheritance. *J. Med. Genet.*, **28**, 79–83.
18. Fischel-Ghodsian,N. (2005) Genetic factors in aminoglycoside toxicity. *Pharmacogenomics*, **6**, 27–36.
19. Bykhovskaya,Y., Mengesha,E., Wang,D., Yang,H., Estivill,X., Shohat,M. and Fischel-Ghodsian,N. (2004) Human mitochondrial transcription factor B1 as a modifier gene for hearing loss associated with the mitochondrial A1555G mutation. *Mol. Genet. Metab.*, **82**, 27–32.
20. Raimundo,N., Song,L., Shutt,T.E., McKay,S.E., Cotney,J., Guan,M.X., Gilliland,T.C., Hohuan,D., Santos-Sacchi,J. and Shadel,G.S. (2012) Mitochondrial stress engages E2F1 apoptotic signaling to cause deafness. *Cell*, **148**, 716–726.
21. Koeck,T., Olsson,A.H., Nitert,M.D., Sharoyko,V.V., Ladenvall,C., Kotova,O., Reiling,E., Ronn,T., Parikh,H., Taneera,J. *et al.* (2011) A common variant in TFB1M is

associated with reduced insulin secretion and increased future risk of type 2 diabetes. *Cell Metab.*, **13**, 80–91.
22. Falkenberg,M., Gaspari,M., Rantanen,A., Trifunovic,A., Larsson,N.G. and Gustafsson,C.M. (2002) Mitochondrial transcription factors B1 and B2 activate transcription of human mtDNA. *Nat. Genet.*, **31**, 289–294.
23. Shutt,T.E., Lodeiro,M.F., Cotney,J., Cameron,C.E. and Shadel,G.S. (2010) Core human mitochondrial transcription apparatus is a regulated two-component system *in vitro*. *Proc. Natl Acad. Sci. USA*, **107**, 12133–12138.
24. Cotney,J. and Shadel,G.S. (2006) Evidence for an early gene duplication event in the evolution of the mitochondrial transcription factor B family and maintenance of rRNA methyltransferase activity in human mtTFB1 and mtTFB2. *J. Mol. Evol.*, **63**, 707–717.
25. McCulloch,V., Seidel-Rogol,B.L. and Shadel,G.S. (2002) A human mitochondrial transcription factor is related to RNA adenine methyltransferases and binds S-adenosylmethionine. *Mol. Cell. Biol.*, **22**, 1116–1125.
26. Shutt,T.E., Lodeiro,M.F., Cotney,J., Cameron,C.E. and Shadel,G.S. (2010) Core human mitochondrial transcription apparatus is a regulated two-component system *in vitro*. *Proc. Natl Acad. Sci. USA*, **107**, 12133–12138.
27. Surovtseva,Y.V. and Shadel,G.S. (2013) Transcription-independent role for human mitochondrial RNA polymerase in mitochondrial ribosome biogenesis. *Nucleic Acids Res.*, **41**, 2479–2488.
28. Cotney,J., McKay,S.E. and Shadel,G.S. (2009) Elucidation of separate, but collaborative functions of the rRNA methyltransferase-related human mitochondrial transcription factors B1 and B2 in mitochondrial biogenesis reveals new insight into maternally inherited deafness. *Hum. Mol. Genet.*, **18**, 2670–2682.
29. O'Farrell,H.C., Musayev,F.N., Scarsdale,J.N., Wright,H.T. and Rife,J.P. (2003) Crystallization and preliminary X-ray diffraction analysis of KsgA, a universally conserved RNA adenine dimethyltransferase in *Escherichia coli*. *Acta Crystallogr. D Biol. Crystallogr.*, **59**, 1490–1492.
30. Kabsch,W. (2010) Xds. *Acta Crystallogr. D Biol. Crystallogr.*, **66**, 125–132.
31. Evans,P. (2006) Scaling and assessment of data quality. *Acta Crystallogr. D Biol. Crystallogr.*, **62**, 72–82.
32. Vonrhein,C., Flensburg,C., Keller,P., Sharff,A., Smart,O., Paciorek,W., Womack,T. and Bricogne,G. (2011) Data processing and analysis with the autoPROC toolbox. *Acta Crystallogr. D Biol. Crystallogr.*, **67**, 293–302.
33. Hendrickson,W.M. and Ogata,C. (1997) Phase determination from multiwavelength anomalous diffraction measurements. *Meth. Enzymol.*, 494–523.
34. Terwilliger,T.C. and Berendzen,J. (1999) Automated MAD and MIR structure solution. *Acta Crystallogr. D Biol. Crystallogr.*, **55**, 849–861.
35. Terwilliger,T.C. (2000) Maximum-likelihood density modification. *Acta Crystallogr. D Biol. Crystallogr.*, **56**, 965–972.
36. Emsley,P. and Cowtan,K. (2004) Coot: model-building tools for molecular graphics. *Acta Crystallogr. D Biol. Crystallogr.*, **60**, 2126–2132.
37. Adams,P.D., Afonine,P.V., Bunkoczi,G., Chen,V.B., Davis,I.W., Echols,N., Headd,J.J., Hung,L.W., Kapral,G.J., Grosse-Kunstleve,R.W. *et al.* (2010) PHENIX: a comprehensive Python-based system for macromolecular structure solution. *Acta Crystallogr. D Biol. Crystallogr.*, **66**, 213–221.
38. Davis,I.W., Leaver-Fay,A., Chen,V.B., Block,J.N., Kapral,G.J., Wang,X., Murray,L.W., Arendall,W.B. 3rd, Snoeyink,J., Richardson,J.S. *et al.* (2007) MolProbity: all-atom contacts and structure validation for proteins and nucleic acids. *Nucleic Acids Res.*, **35**, W375–W383.
39. Strong,M., Sawaya,M.R., Wang,S., Phillips,M., Cascio,D. and Eisenberg,D. (2006) Toward the structural genomics of complexes: crystal structure of a PE/PPE protein complex from Mycobacterium tuberculosis. *Proc. Natl Acad. Sci. USA*, **103**, 8060–8065.
40. Baba,T., Ara,T., Hasegawa,M., Takai,Y., Okumura,Y., Baba,M., Datsenko,K.A., Tomita,M., Wanner,B.L. and Mori,H. (2006) Construction of *Escherichia coli* K-12 in-frame, single-gene knockout mutants: the Keio collection. *Mol. Syst. Biol.*, **2**, 2006.0008.
41. van Buul,C.P. and van Knippenberg,P.H. (1985) Nucleotide sequence of the ksgA gene of *Escherichia coli*: comparison of methyltransferases effecting dimethylation of adenosine in ribosomal RNA. *Gene*, **38**, 65–72.
42. Claros,M.G. and Vincens,P. (1996) Computational method to predict mitochondrially imported proteins and their targeting sequences. *Eur. J. Biochem.*, **241**, 779–786.
43. Kabsch,W. and Sander,C. (1983) Dictionary of protein secondary structure: pattern recognition of hydrogen-bonded and geometrical features. *Biopolymers*, **22**, 2577–2637.
44. Schluckebier,G., Zhong,P., Stewart,K.D., Kavanaugh,T.J. and Abad-Zapatero,C. (1999) The 2.2 A structure of the rRNA methyltransferase ErmC' and its complexes with cofactor and cofactor analogs: implications for the reaction mechanism. *J. Mol. Biol.*, **289**, 277–291.
45. Yakubovskaya,E., Guja,K.E., Mejia,E., Castano,S., Hambardjieva,E., Choi,W.S. and Garcia-Diaz,M. (2012) Structure of the essential MTERF4:NSUN4 protein complex reveals how an MTERF protein collaborates to facilitate rRNA modification. *Structure*, **20**, 1940–1947.
46. Fislage,M., Roovers,M., Tuszynska,I., Bujnicki,J.M., Droogmans,L. and Versees,W. (2012) Crystal structures of the tRNA:m2G6 methyltransferase Trm14/TrmN from two domains of life. *Nucleic Acids Res.*, **40**, 5149–5161.
47. Schluckebier,G., Kozak,M., Bleimling,N., Weinhold,E. and Saenger,W. (1997) Differential binding of S-adenosylmethionine S-adenosylhomocysteine and Sinefungin to the adenine-specific DNA methyltransferase M.TaqI. *J. Mol. Biol.*, **265**, 56–67.
48. Vidgren,J., Svensson,L.A. and Liljas,A. (1994) Crystal structure of catechol O-methyltransferase. *Nature*, **368**, 354–358.
49. Martin,J.L. and McMillan,F.M. (2002) SAM (dependent) I AM: the S-adenosylmethionine-dependent methyltransferase fold. *Curr. Opin. Struct. Biol.*, **12**, 783–793.
50. Li,L., Li,C., Sarkar,S., Zhang,J., Witham,S., Zhang,Z., Wang,L., Smith,N., Petukh,M. and Alexov,E. (2012) DelPhi: a comprehensive suite for DelPhi software and associated resources. *BMC Biophys.*, **5**, 9.
51. Tu,C., Tropea,J.E., Austin,B.P., Court,D.L., Waugh,D.S. and Ji,X. (2009) Structural basis for binding of RNA and cofactor by a KsgA methyltransferase. *Structure*, **17**, 374–385.
52. O'Farrell,H.C., Scarsdale,J.N. and Rife,J.P. (2004) Crystal structure of KsgA, a universally conserved rRNA adenine dimethyltransferase in *Escherichia coli*. *J. Mol. Biol.*, **339**, 337–353.
53. Schubot,F.D., Chen,C.J., Rose,J.P., Dailey,T.A., Dailey,H.A. and Wang,B.C. (2001) Crystal structure of the transcription factor sc-mtTFB offers insights into mitochondrial transcription. *Protein Sci.*, **10**, 1980–1988.
54. Pulicherla,N., Pogorzala,L.A., Xu,Z., O Farrell,H.C., Musayev,F.N., Scarsdale,J.N., Sia,E.A., Culver,G.M. and Rife,J.P. (2009) Structural and functional divergence within the Dim1/KsgA family of rRNA methyltransferases. *J. Mol. Biol.*, **391**, 884–893.
55. Bussiere,D.E., Muchmore,S.W., Dealwis,C.G., Schluckebier,G., Nienaber,V.L., Edalji,R.P., Walter,K.A., Ladror,U.S., Holzman,T.F. and Abad-Zapatero,C. (1998) Crystal structure of ErmC', an rRNA methyltransferase which mediates antibiotic resistance in bacteria. *Biochemistry*, **37**, 7103–7112.
56. Schluckebier,G., Zhong,P., Stewart,K.D., Kavanaugh,T.J. and Abad-Zapatero,C. (1999) The 2.2 A structure of the rRNA methyltransferase ErmC' and its complexes with cofactor and cofactor analogs: implications for the reaction mechanism. *J. Mol. Biol.*, **289**, 277–291.
57. Menezes,S., Gaston,K.W., Krivos,K.L., Apolinario,E.E., Reich,N.O., Sowers,K.R., Limbach,P.A. and Perona,J.J. (2011) Formation of m2G6 in Methanocaldococcus jannaschii tRNA catalyzed by the novel methyltransferase Trm14. *Nucleic Acids Res.*, **39**, 7641–7655.
58. Demirci,H., Belardinelli,R., Seri,E., Gregory,S.T., Gualerzi,C., Dahlberg,A.E. and Jogl,G. (2009) Structural rearrangements in the active site of the *Thermus thermophilus* 16S rRNA

methyltransferase KsgA in a binary complex with 5′-methylthioadenosine. *J. Mol. Biol.*, **388**, 271–282.
59. Maravic,G., Bujnicki,J.M., Feder,M., Pongor,S. and Flogel,M. (2003) Alanine-scanning mutagenesis of the predicted rRNA-binding domain of ErmC' redefines the substrate-binding site and suggests a model for protein-RNA interactions. *Nucleic Acids Res.*, **31**, 4941–4949.
60. Buriankova,K., Doucet-Populaire,F., Dorson,O., Gondran,A., Ghnassia,J.C., Weiser,J. and Pernodet,J.L. (2004) Molecular basis of intrinsic macrolide resistance in the Mycobacterium tuberculosis complex. *Antimicrob. Agents chemother.*, **48**, 143–150.
61. Schinkel,A.H., Koerkamp,M.J., Touw,E.P. and Tabak,H.F. (1987) Specificity factor of yeast mitochondrial RNA polymerase. Purification and interaction with core RNA polymerase. *J. Biol. Chem.*, **262**, 12785–12791.
62. Dunkle,J.A., Xiong,L., Mankin,A.S. and Cate,J.H. (2010) Structures of the *Escherichia coli* ribosome with antibiotics bound near the peptidyl transferase center explain spectra of drug action. *Proc. Natl Acad. Sci. USA*, **107**, 17152–17157.
63. McClelland,M. (1981) Purification and characterization of two new modification methylases: MClaI from Caryophanon latum L and MTaqI from Thermus aquaticus YTI. *Nucleic Acids Res.*, **9**, 6795–6804.
64. Goedecke,K., Pignot,M., Goody,R.S., Scheidig,A.J. and Weinhold,E. (2001) Structure of the N6-adenine DNA methyltransferase M.TaqI in complex with DNA and a cofactor analog. *Nat. Struct. Biol.*, **8**, 121–125.
65. Pues,H., Bleimling,N., Holz,B., Wolcke,J. and Weinhold,E. (1999) Functional roles of the conserved aromatic amino acid residues at position 108 (motif IV) and position 196 (motif VIII) in base flipping and catalysis by the N6-adenine DNA methyltransferase from Thermus aquaticus. *Biochemistry*, **38**, 1426–1434.
66. Boehringer,D., O'Farrell,H.C., Rife,J.P. and Ban,N. (2012) Structural insights into methyltransferase KsgA function in 30S ribosomal subunit biogenesis. *J. Biol. Chem.*, **287**, 10453–10459.
67. Richter,U., Kuhn,K., Okada,S., Brennicke,A., Weihe,A. and Borner,T. (2010) A mitochondrial rRNA dimethyladenosine methyltransferase in Arabidopsis. *Plant J.*, **61**, 558–569.
68. Adan,C., Matsushima,Y., Hernandez-Sierra,R., Marco-Ferreres,R., Fernandez-Moreno,M.A., Gonzalez-Vioque,E., Calleja,M., Aragon,J.J., Kaguni,L.S. and Garesse,R. (2008) Mitochondrial transcription factor B2 is essential for metabolic function in Drosophila melanogaster development. *J. Biol. Chem.*, **283**, 12333–12342.
69. Matsushima,Y., Garesse,R. and Kaguni,L.S. (2004) Drosophila mitochondrial transcription factor B2 regulates mitochondrial DNA copy number and transcription in schneider cells. *J. Biol. Chem.*, **279**, 26900–26905.
70. Matsushima,Y., Adan,C., Garesse,R. and Kaguni,L.S. (2005) Drosophila mitochondrial transcription factor B1 modulates mitochondrial translation but not transcription or DNA copy number in Schneider cells. *J. Biol. Chem.*, **280**, 16815–16820.
71. Goedecke,K., Pignot,M., Goody,R.S., Scheidig,A.J. and Weinhold,E. (2001) Structure of the N6-adenine DNA methyltransferase M.TaqI in complex with DNA and a cofactor analog. *Nat. Struct. Biol.*, **8**, 121–125.
72. Klimasauskas,S., Kumar,S., Roberts,R.J. and Cheng,X. (1994) HhaI methyltransferase flips its target base out of the DNA helix. *Cell*, **76**, 357–369.
73. Allan,B.W., Beechem,J.M., Lindstrom,W.M. and Reich,N.O. (1998) Direct real time observation of base flipping by the EcoRI DNA methyltransferase. *J. Biol. Chem.*, **273**, 2368–2373.
74. Cheng,X. and Roberts,R.J. (2001) AdoMet-dependent methylation, DNA methyltransferases and base flipping. *Nucleic Acids Res.*, **29**, 3784–3795.